Optics Letters

Beyond GHz optical frequency up-converted modulation of LEDs with integrated acousto-optic transducer

Li-Chan Lai, Dai-Jie Lin, Wen-Hao Chiang, Cheng-Ting Huang, Gong-Ru Lin, and Jian-Jang Huang*

The Graduate Institute of Photonics and Optoelectronics, National Taiwan University, No. 1, Roosevelt Road, Sec. 4, Taipei 106, Taiwan
**Corresponding author: jjhuang@ntu.edu.tw*

Received 18 August 2021; revised 16 September 2021; accepted 18 September 2021; posted 23 September 2021 (Doc. ID 440983); published 11 October 2021

Traditional visible light communication (VLC) via light-emitting diodes (LEDs) employs the on-off keying (OOK) modulation scheme. Even though optical frequency modulation has many advantages, it is hardly used for LED VLC because a high carrier frequency cannot be applied to the LED cavity due to the resistance-capacitance limit. Here, by monolithically integrating an LED with an integrated digital transducer, we experimentally demonstrate the intermixing of gigahertz surface acoustic waves and electrical data signals in the LED cavity at room temperature. An optical transmitter was realized by *in situ* frequency up-conversion of the data signals from an LED, which has the advantages of improving transmission performance by up-shifting the data spectrum away from low-frequency noise. Our proposed integrated acousto-optic transducer opens a new developing scheme on the frequency up-mixed data encoding of an LED beyond its inherent modulation bandwidth for future VLC.

https://doi.org/10.1364/OL.440983

Visible light communication (VLC) has been widely explored in the past several years because of the emerging demands on high security, high spatial reuse, and electromagnetic interference-free and license-free networks [1–3]. Excellent frequency bandwidth can be achieved from LEDs (light-emitting diodes) using single quantum-well structures [3,4], non-polar or semi-polar light-emitting materials [5,6], distributed Bragg reflection (DBR) structures [7], micro-scale emitting areas [8], quantum dots [8], and photonic crystals [9,10]. Most of the above approaches utilized the on-off keying (OOK) modulation technique [3–5,8–10], a communication protocol commonly used for optical modulation.

On the other hand, optical frequency modulation has been studied using semiconductor lasers [11–15]. Optical frequency modulation has the advantages of a higher bandwidth, a better signal quality, and lower noise over the typical OOK modulation technique. However, literature surveys show that this technology was rarely reported from the spontaneous LED light sources because the carrier frequency is limited by the resistance-capacitance effect (RC).

We previously demonstrated optical oscillation in the GHz frequency range by exerting surface acoustic waves (SAWs) on an LED [16,17]. The GHz oscillation is the harmonics of the SAWs excited by the integrated digital transducer (IDT). Only the harmonic frequency bands that fall within the thickness vibration modes of the LED cavity can be optically detected [17]. The acousto-optic (AO) interaction generates high-frequency optical oscillation, which cannot be observed from typical electrical excitation on the LEDs due to the RC limit.

This work demonstrates that the electrical data signal (in the sub-100 MHz range) can be intermixed with the GHz acoustic excitation in the LED cavity, which leads to an effect of frequency up-conversion. We further applied such a phenomenon to optical data transmission at room temperature. The proposed AO frequency up-converted modulation has the advantage of suppressing low-frequency noise to ensure a high signal-to-noise ratio (SNR) over a long traveling distance as compared with conventional OOK modulation.

In this work, devices for signal transmission are composed of a lateral LED and an IDT. They are integrated monolithically on the sapphire substrate (see Fig. 1). Our previous work [16], refers to a detailed material structure and a device fabrication process for radio frequency-modulated light emitters. In this paper, the light-emitting mesa area is $100 \times 100\ \mu m^2$, and the IDT is located on the n-type GaN layer. The excited SAWs propagate laterally toward the LED, as illustrated in Fig. 1. The IDT consists of 15 fingers with the length of 516 μm and the width of 5.5 μm. The spacing between fingers is 5.5 μm. The IDT and the LED are 336 μm apart from each other.

To understand the quality of data transmission by frequency up-conversion, device properties as well as the system performance were benchmarked. First, we characterized SAW harmonic frequencies from the IDT. Second, SAW harmonics generated from the IDT were fed into the LED, and the corresponding spectrum of the optical response was measured. Third, the optical spectra of the LED, by coupling the electrical data signals with the acoustic vibration modes in the LED cavity, were extracted. This measurement demonstrates a frequency

up-conversion of the signals by the acoustic waves (carrier frequency). Fourth, data transmissions with and without up-conversion were characterized by comparing their eye diagrams at different optical traveling distances. All the measurements were operated at room temperature.

In the first experiment, to measure the harmonics of the SAWs, we prepared a sample with two IDTs 293 μm apart from each other. Square-wave signals from a pulse pattern generator (PPG) (Anritsu MP1652A) were applied to one IDT. The generated acoustic signals traveled toward the second IDT and were then converted back to electrical waveforms. A spectral analyzer, Tektronix RSA306B, was employed to record the SAW harmonics.

Second, using a sample with an LED integrated with an acoustic transducer, as illustrated in Fig. 1, a high-speed photodetector (Newport 1601FC-AC with a frequency bandwidth of 1 GHz) was placed right on top of the LED to detect the optical signal. The spectrum was then read out from the spectral analyzer. During the measurement, the LED was biased at a constant injection current of 100 mA.

As for the third experiment, we performed frequency mixing of the acoustic and the electrical signals using the setup shown in Fig. 2 (framed by a red line). An electrical signal with a data rate of 20 Mbps from a function generator (Aligent 33220 A) was fed into the LED. The data is in a sinusoidal waveform. Meanwhile, the SAWs were propagated toward the LED by applying square-wave electrical excitation on the IDT. Light output, mixed with the data signal and SAW harmonic modes, was received by the photodetector (Newport 1601FC-AC) through a 0.8 m-in- length plastic optical fiber. The spectrum of up-converted signals was than extracted by a spectrum analyzer (Tektronix RSA306B) using a high pass filter.

In the fourth measurement, the optical up-link and down-link transmission was conducted with the setup encompassed in the green line in Fig. 2. An electrical signal with a data rate of 100 Mbps was applied to the LED by an arbitrary waveform generator (Tektronix 7122B). The frequency up-converted lightwave traveled through the plastic fiber of different lengths. The detected optical signal was then down-converted by a mixer with a frequency of 1250 MHz. In this experiment, a high-pass filter (HPF) and a low-pass filter (LPF) were placed adjacant to the mixer. The HPF removes low-frequency noise less than 1 GHz, while the LPF filters out the higher but unnecessary frequency components over 1 GHz after passing through the mixer.

We first demonstrate the frequency modes of the SAWs that are available from exciting the IDT. The spectrum was extracted from the second IDT, as shown in Fig. 3(a). With the square

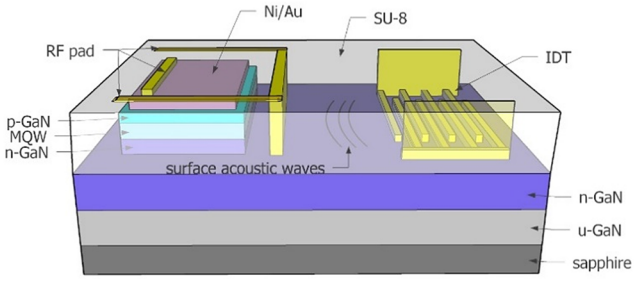

Fig. 1. Top view of the integrated AO transducer, which consists of an LED and an IDT. The SAWs propagate through the n-type GaN once actuated.

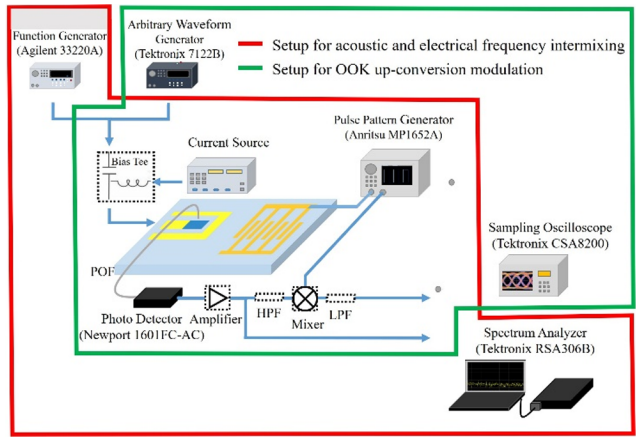

Fig. 2. Setup for (i) acoustic and electrical frequency intermixing (red line) and (ii) optical transmission of the up-converted data signals by the SAWs (green line).

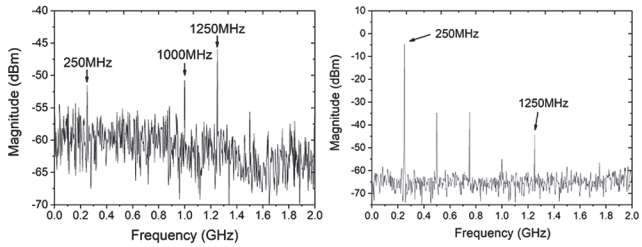

Fig. 3. (a) Harmonics of the SAWs under the 250 MHz electrical excitation. The harmonics were extracted from the second IDT by converting the acoustic waves to electrical signals. (b) Optical output spectrum from the LED under the 250 MHz IDT excitation.

wave electrical input excitation of 250 MHz, frequency multiplies at 500, 750, 1000, and 1250 MHz are observed. Since the metallization ratio is around 0.5 for our "solid-electrode" (two-finger) IDT structure, the odd-harmonic frequency responses, 750 (3rd order) and 1250 MHz (5th order), have a higher magnitude than the even harmonics [18].

In the second measurement, when we applied a square wave electrical signal with a frequency of 250 MHz to the IDT, the SAW harmonics propagated toward the LED, which resulted in an optical output with the resonant frequencies of 250, 1000, and 1250 MHz shown in Fig. 3(b). Among them, 250 MHz is the fundamental SAW frequency, while 1000 and 1250 MHz are the SAW harmonics that fall within the resonance (thickness vibration modes) of the LED due to the AO interaction [16,17]. Because the quantum wells within the LED vibrate and thus the energy band fluctuates with the harmonics of acoustic excitation, light output oscillates with the SAW harmonics.

Next, following the experimental setup in Fig. 2 for frequency intermixing, we applied a square electrical waveform with the excitation frequency of 250 MHz to the IDT and digital data signals of 20 MHz to the LED. The digital data signal frequency is below the 3-dB small-signal optical frequency response of around 240 MHz, which was extracted by injecting 100 mA DC current into the LED in a separate measurement. Frequency mixing was observed in the optical output because the quantum wells experienced vibration of energy bands as well as on-off carrier injection. In such a measurement, we deliberately chose

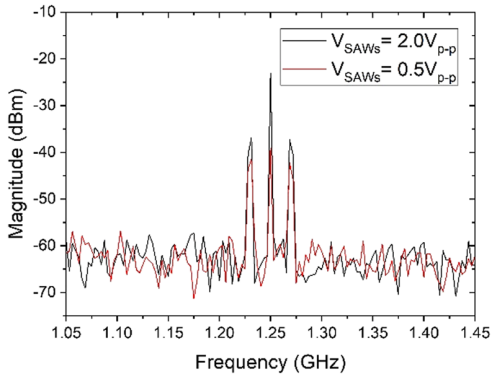

Fig. 4. Optical output spectra under the IDT driving voltage of 0.5 and 2 V_{p-p}.

1250 MHz as the carrier frequency because its SAW magnitude is higher than that of 1000 MHz. The SAW harmonics at the rest of the frequencies were removed by the HPF and LPF. In Fig. 4, for an IDT driven at either 0.5 or 2 V_{p-p} (peak-to-peak voltage), the optical output spectrum within the acoustic resonant range of 1250 MHz is composed of three peaks. The center one is the carrier frequency of 1250 MHz while the sidebands are the mixing of the carrier frequency and the data signal. It suggests the up-conversion of data signals by SAW excitation in the LED cavity. From the Bessel and trigonometric functions of narrowband frequency-shifting signals [19], considering only the first pair of sidebands, the upconverted modulated signal, $S_{FS,modulated}$ is written as

$$S_{FS,modulated}(t) = A_{SAWs}\cos(2\pi f_{SAWs}t) + \frac{A_{SAWs}A_m}{2}\cos(2\pi(f_{SAWs}+f_m)t) + \frac{A_{SAWs}A_m}{2}\cos(2\pi(f_{SAWs}-f_m)t), \quad (1)$$

where A_{SAWs} and A_m are the relative magnitude of the SAW and the data signal, and f_{SAWs} and f_m are the frequency of the SAW and the data signal. The sidebands at 1250 ± 20 MHz in Fig. 4 are attributed to the modulation by the SAWs in the LED, following Eq. (1). For the SAW-modulated LED, the frequency mixing occurs when the mechanical resonant mode and the electrical signal from the LED cavity are actuated, which results in the Raman scattering of the intracavity optical field [19–21]. The inelastic Stokes and anti-Stokes scattering processes in the InGaN/GaN quantum wells generate three frequency bands in Fig. 4 [22].

To understand how the SAW excitation affects the transmission quality, in Fig. 4 we compare the frequency-domain optical spectra at two different peak-to-peak voltages (V_{p-p}). At 2 V_{p-p}, the sideband peaks at ±20 MHz are around 5.29 dB higher than that driving at 0.5 V_{p-p}. The corresponding SNR increases from 16.45 to 23.07 dB. The results can be understood from Eq. (1), which shows that $S_{FS,modulated}$ is proportional to the intensity of acoustic signals. It also suggests that when the correlation between IDT driving voltage and the generated acoustic magnitude is linear, a higher IDT driving is preferred to increase the SNR of the transmitted optical signal. In the subsequent experiment, 2 V_{p-p} was chosen for IDT bias.

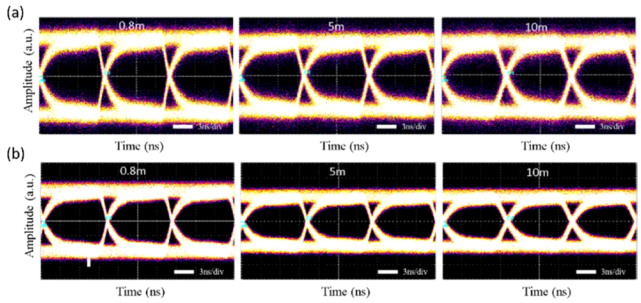

Fig. 5. Evaluated eye diagrams (a) with up-conversion and (b) without up-conversion. The data rate is 100 Mbps. The traveling length within the plastic fiber is 0.8, 5, and 10 m from left to right.

Following the measurement setup for the frequency up-conversion, we next applied the on-off keying (OOK) modulation scheme to the LED. The LED injection current is 100 mA, with the data signal amplitude of 2 V_{p-p}. The voltage applied to the IDT is also 2 V_{p-p}. The up-converted optical OOK signals travel through the fiber over a distance of 0.8, 5, and 10 m before a high-speed detector converts them back to electrical waveforms. For comparison, the conventional OOK approach was also conducted with the same measurement setup for frequency up-conversion but with the HPF and mixer removed. The eye diagrams are shown in Fig. 5 along with the results without the up-conversion process (the conventional OOK approach). Because optical waves traveling through the fiber suffer from fiber bending loss, scattering, absorption, and dispersion, the receiving optical intensity decreases with the increase of the fiber length. The signal intensity in the eye diagram of the up-converted modulation is lower than that of the non-converted case because of the energy loss during frequency conversion and bandpass filtering. The higher intensity of the direct data transmission may not be preferred as it is also attributed to the excess but spurious signal energy, known as low-frequency noise [23]. Despite a slightly lower intensity level for the up-converted signal, the Root Mean Square (RMS) jitter, defined as the standard deviation of the associated Gaussian distribution, is 157.81 ps. It is lower than that of the conventional OOK method of 216.34 ps when the fiber length is 0.8 m. When the fiber length increases to 10 m, the RMS jitter of the up-converted signal is 118.30 ps, which is 54.32 ps lower than the conventional OOK method. The superior performance of the up-conversion is attributed to filtering out the random jitter arising from the thermal and shot noise at low frequency [24,25].

The corresponding SNRs of the received data are shown in Fig. 6, indicating that more than 1.5 dB of the SNR enhancement can be achieved through all distances in the plastic-optic fiber channel. Because of such an *in situ* frequency up-converted modulation via the integrated AO transducer, the data transmission performance is improved by up-shifting the data spectrum away from low-frequency noise, including the flicker (1/f) noise, the clock drift, and other environmental noises. Although the up-conversion cannot overcome the inherent nature of SNR degradation by around 1.15 dB with increasing distance of propagation up to 10 m, our work indicates a new method of visible light communication by monolithically integrating an LED with an IDT for better transmission quality over a long traveling distance.

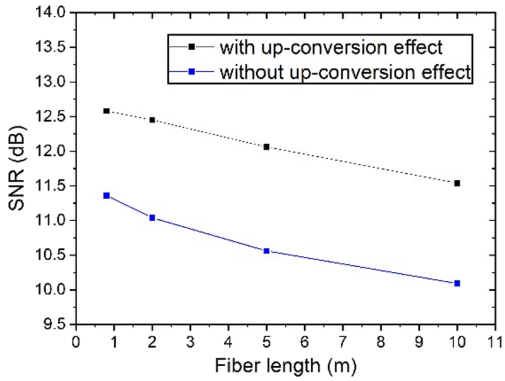

Fig. 6. SNR versus signal traveling length in the fiber with and without up-conversion.

In summary, gigahertz frequency up-conversion of the data signals was realized with the assistance of the SAW excited resonance within the LED cavity. Because of such an *in situ* frequency up-converted modulation via the integrated AO transducer, the data transmission performance is improved by up-shifting the data spectrum away from the low-frequency noise. Our work declares a new LED scheme for elevating the receiving performance significantly, which establishes a new era in developing frequency up-mixed data encoding of LEDs beyond its inherent optical bandwidth for future visible light communication.

Funding. Ministry of Science and Technology, Taiwan (108-2221-E-002-014-MY3).

Disclosures. The authors declare no conflicts of interest.

Data Availability. Data underlying the results presented in this Letter are not publicly available at this time but may be obtained from the authors upon reasonable request.

REFERENCES

1. H. Burchardt, N. Serafimovski, D. Tsonev, S. Videv, and H. Haas, IEEE Commun. Mag. **52**, 98 (2014).
2. H. Elgala, R. Mesleh, and H. Haas, IEEE Commun. Mag. **49**, 56 (2011).
3. T.-C. Lin, Y.-T. Chen, Y.-F. Yin, Z.-X. You, H.-Y. Kao, C.-Y. Huang, Y.-H. Lin, C.-T. Tsai, G.-R. Lin, and J.-J. Huang, IEEE Trans. Electron Device **65**, 4375 (2018).
4. H.-Y. Lan, I.-C. Tseng, Y.-H. Lin, G.-R. Lin, D.-W. Huang, and C.-H. Wu, Opt. Lett. **45**, 2203 (2020).
5. S.-W. H. Chen, Y.-M. Huang, Y.-H. Chang, Y. Lin, F.-J. Liou, Y.-C. Hsu, J. Song, J. Choi, C.-W. Chow, C.-C. Lin, R.-H. Horng, Z. Chen, J. Han, T. Wu, and H.-C. Kuo, ACS Photon. **7**, 2228 (2020).
6. A. Rashidi, M. Monavarian, A. Aragon, S. Okur, M. Nami, A. Rishinaramangalam, S. Mishkat-Ul-Masabih, and D. Feezell, IEEE Photon. Technol. Lett. **29**, 381 (2017).
7. X. Ding, C. Gui, H. Hu, M. Liu, X. Liu, J. Lv, and S. Zhou, Appl. Opt. **56**, 4375 (2017).
8. S. Mei, X. Liu, W. Zhang, R. Liu, L. Zheng, R. Guo, and P. Tian, ACS Appl. Mater. Interfaces **10**, 5641 (2018).
9. Y. F. Yin, W. Y. Lan, Y. H. Hsu, Y. F. Hsu, C. H. Wu, and J. J. Huang, J. Appl. Phys. **119**, 013103 (2016).
10. Y. F. Yin, W. Y. Lan, T. C. Lin, C. Wang, M. Feng, and J. J. Huang, J. Lightwave Technol. **35**, 258 (2017).
11. S.-K. Hwang, J.-M. Liu, and J. K. White, IEEE J. Sel. Top. Quantum Electron. **10**, 974 (2004).
12. X. Lin, G. Xia, Z. Shang, T. Deng, X. Tang, L. Fan, Z. Gao, and Z. Wu, Opt. Express **27**, 1217 (2019).
13. C.-H. Tseng, Y.-H. Hung, and S.-K. Hwang, Opt. Lett. **44**, 3334 (2019).
14. J.-P. Zhuang, X.-Z. Li, S.-S. Li, and S.-C. Chan, Opt. Lett. **41**, 5764 (2016).
15. P. Zhou, F. Zhang, and S. Pan, J. Lightwave Technol. **36**, 3927 (2018).
16. M.-Y. Tsai, S.-Y. Pan, and J.-J. Huang, IEEE Trans. Ultrason. Ferroelectr. Freq. Control **68**, 854 (2021).
17. M.-Y. Tsai, L.-C. Lai, and J.-J. Huang, IEEE Trans. Ultrason. Ferroelectr. Freq. Control **68**, 1949 (2021).
18. C. K. Campbell, *Surface Acoustic Wave Devices for Mobile and Wireless Communications* (Academic, 1998), pp. 186–187.
19. A. Maskay, D. M. Hummels, and M. P. Da Cunha, IEEE Trans. Ultrason. Ferroelectr. Freq. Control **66**, 91 (2019).
20. S. Tallur and S. A. Bhave, IEEE Photon. J. **4**, 1474 (2012).
21. M. Weiß, D. Wigger, M. Nägele, K. Müller, J. J. Finley, T. Kuhn, P. Machnikowski, and H. J. Krenner, Optica **8**, 291 (2021).
22. J. Wagner, A. Ramakrishnan, H. Obloh, and M. Maier, Appl. Phys. Lett. **74**, 3863 (1999).
23. M. Baker, *Demystifying Mixed Signal Test Methods*, M. Baker, ed. (Newnes, 2003), pp. 115–146.
24. A. Van Der Ziel and E. R. Chenette, *Advances in Electronics and Electron Physics*, L. Marton, ed. (Academic, 1978), pp. 313–383.
25. N. Ren, Z. Fu, S. Lei, H. Liu, and S. Tian, Electronics **8**, 1510 (2019).